Two-Phase Convection Heat Transfer Correlations for Liquid Hydrogen Pipe Chilldown

Samuel R. Darr[1] and Jason W. Hartwig[2]

[1]The Aerospace Corporation, El Segundo, CA, USA
[2]NASA Glenn Research Center, Cleveland, OH, USA

Corresponding Author: Samuel R. Darr
M/S: M4-965
2310 E El Segundo Blvd, El Segundo, CA, 90245, USA
samuel.r.darr@aero.org
Phone: 310-336-5834

ABSTRACT:

Recently, heat transfer correlations based on liquid nitrogen (LN_2) and liquid hydrogen (LH_2) pipe quenching data were developed to improve the predictive accuracy of lumped node codes like SINDA/FLUINT and the Generalized Fluid System Simulation Program (GFSSP). After implementing these correlations into both programs, updated model runs showed strong improvement in LN_2 pipe chilldown modeling but only modest improvement in LH_2 modeling. Due to large differences in thermal and fluid properties between the two fluids, results indicated a need to develop a separate set of LH_2-only correlations to improve the accuracy of the simulations. This paper presents a new set of two-phase convection heat transfer correlations based on LH_2 pipe quenching data. A correlation to predict the bulk vapor temperature was developed after analysis showed that high amounts of thermal nonequilibrium of the liquid and vapor phases occurred during film boiling of LH_2. Implemented in a numerical model, the new correlations achieve a mean absolute error of 19.5 K in the predicted wall temperature when compared to recent LH_2 pipe chilldown data, an improvement of 40% over recent GFSSP predictions. This correlation set can be implemented in simulations of the transient LH_2 chilldown process. Such simulations are useful for predicting the chilldown time and boil-off mass of LH_2 for applications such as the transfer of LH_2 from a ground storage tank to the rocket vehicle propellant tank, or through a rocket engine feedline during engine startup.

Keywords

Cryogenic pipe chilldown, liquid hydrogen, two-phase flow, quenching

Nomenclature

c_p	specific heat capacity at constant pressure [J/kg-K]
D	inner diameter of tube [m]
G	mass flux [kg/m^2-s]
g	gravity [m/s^2]
h	heat transfer coefficient [W/m^2-K]
hfg	heat of vaporization [J/kg]
Ja	Jakob number, $c_p(T_w - T_{sat})/h_{fg}$
k	thermal conductivity [W/m-K]

K	fitting parameter in quality calculation
L	length from quenching front [m]
Nu	Nusselt number, hD/k
P	pressure [Pa]
Pr	Prandtl number, $c_p\mu/k$
q''	heat flux [W/m^2]
Re	Reynolds number, GD/μ
Re_{tp}	two-phase Reynolds number, $GDx_a/(\alpha\mu_{v,f})$
T	temperature [K]
We_D	Weber number, $G^2D/(\rho\gamma)$
x_a	actual quality
x_e	equilibrium quality

Greek

α	vapor volume fraction
γ	surface tension [N/m]
μ	dynamic viscosity [Pa-s]
ρ	density [kg/m^3]

Subscripts

cr	at the critical state
DB	Dittus-Boelter
DF	dispersed flow
DNB	at the departure of nucleate boiling
fb	film boiling
f	at the film temperature
IAF	inverted annular flow
l	liquid
NB	nucleate boiling
sat	at the saturation state
SP	single-phase
TB	transition boiling
v	bulk vapor
w	wall
wet	at the rewet temperature, or Leidenfrost temperature

1 Introduction

The transfer of cryogenic propellant through a pipe that is initially at room temperature results in a two-phase flow boiling process that ensues until the pipe is cooled to the liquid temperature. Generally, the flow starts in a film boiling regime, in which the wall is above the Leidenfrost temperature, and passes through the reverse boiling curve from film boiling to transition boiling to nucleate boiling to single-phase liquid convection. At the initial high wall temperatures, the pipe wall is covered by a vapor blanket, and any approaching liquid evaporates entirely or is pushed away by the propulsive force of evaporation before touching the wall. Once the pipe is cooled to the Leidenfrost temperature, the liquid sporadically touches the wall, such that a chaotic mixture of film and nucleate boiling occurs on the surface. At the temperature corresponding to the critical

heat flux, the liquid can make full contact with the wall and the flow is in the nucleate boiling regime. The pipe will continue to cool past the onset of nucleate boiling. Below this temperature, the wall superheat is too low to sustain nucleate boiling, and the only mode of heat transfer is single-phase liquid convection.

In recent years, there has been a growing interest in the prediction of the heat transfer during cryogenic pipe chilldown. For a detailed description of previous experiments and correlation development prior to 2016, the reader is referred to (Darr et al. 2019). Hartwig et al. (2016) compared existing film boiling, nucleate boiling, and critical heat flux (CHF) correlations available in the literature against liquid hydrogen (LH_2) and liquid nitrogen (LN_2) chilldown data. It was determined that many of that existing correlations over-predicted heat transfer and that significant model improvements were warranted. Darr et al. (2015) developed a set of cryogenic pipe chilldown heat transfer correlations fit to LN_2 data with the flow oriented downward in the same direction as gravity. A numerical model that implemented the new correlations was able to predict the transient pipe wall temperature with good accuracy. Darr et al. (2016b) provided an updated version of these correlations for LN_2 pipe chilldown data in 9 different directions with respect to gravity (experiment described in Darr et al. 2016a). Jin et al. (2018) compared some existing correlations against recently conducted low-Reynolds LN_2 data and found good agreement over the range of 26 – 74 kg/m^{2}s. Singh et al. (2019) also recently compared flow visualization with void fraction predictions for LN_2 chilldown. Darr et al. (2019a) provided a new set of cryogenic chilldown correlations that was fit to both LH_2 and LN_2 data. These latest correlations were implemented into the lumped-node codes SINDA/FLUINT and the Generalized Fluid System Simulation Program (GFSSP) to predict the pipe wall temperature during chilldown (Sakowski et al. 2018, Leclair et al. 2018). After implementing the correlations from Darr et al. (2019a) into both programs, results showed strong improvement in LN_2 pipe chilldown modeling but only modest improvement in LH_2 modeling. For LH_2, the correlations generally underpredicted the experimental data, so that the time for the pipe to cool to the liquid temperature was predicted to take longer than the test. The proposed reason for this discrepancy that this paper puts forward is that the correlations from Darr et al. (2019a) do not correctly model the relationship between the wall-to-fluid heat flux and the quality at medium to high quality flows.

In the paper comparing GFSSP results to data, the best results for LH_2 were achieved by using the single-phase Dittus-Boelter heat transfer correlation for the entire boiling regime (Leclair et al. 2018). This is most likely because most of the pipe is in the single-phase vapor regimes during chilldown. At the start of pipe chilldown, there is a high heat flux near the entrance of the tube that quickly brings the quality of the flow towards a value of one before it reaches a far distance down the pipe. Nucleate boiling or transition boiling is sustainable only at low superheat levels, so the vast majority of time is spent in either single-phase vapor convection or film boiling. This is supported by flow visualization of the NASA GRC LH_2 tests, which do not show liquid droplets in the flow until the pipe is nearly chilled down to the liquid temperature (Hartwig and Styborski). Chi and Vetere (1964) performed LH_2 pipe chilldown experiments and reported that at a location roughly one foot downstream of the inlet the vapor and mist flow persisted for the major portion of the time to cool the downstream portion of the pipe to the liquid temperature.

Another reason that the Dittus-Boelter correlation was successful is that the convection heat transfer rates between the liquid and vapor phases are very similar for LH_2 because of the similarity

in the vapor and liquid properties, whereas the difference in properties for other cryogenic fluids like nitrogen, oxygen, and methane is quite large. Single phase heat transfer coefficients (HTCs) using the Dittus-Boelter correlation, normalized by the max value, are calculated for cryogenic fluids in Figure 1 for different values of the fluid temperature. For each fluid, there is a discontinuity in the HTC at the saturation temperature. At temperatures below this value, the fluid is a liquid and the HTC is calculated with liquid properties. Above this temperature, the fluid is a vapor and the HTC is calculated with vapor properties. For example, the figure shows that the HTC decreases from the maximum value at a liquid temperature of 80 K to about 50% of the maximum value at a vapor temperature of 81 K. For hydrogen and helium, the single-phase liquid HTC is smaller than the single-phase gas HTC. For nitrogen, oxygen, and methane, the HTC is larger for liquid than gas. Rearranging the Dittus-Boelter correlation below reveals the effect of each fluid property on the single-phase HTC. The specific heat of LH_2 and liquid helium is smaller than their corresponding vapor specific heats. Whereas, for nitrogen, oxygen, and methane the specific heat is much larger for the liquid than the vapor. Additionally, the ratio of $k^{0.6}/\mu^{0.4}$ is smaller for LH_2 and liquid helium than the corresponding vapors. The reverse is true for nitrogen, oxygen, and methane.

$$h = 0.023 Re^{0.8}\, Pr^{0.4} \left(\frac{k}{D}\right) = 0.023 \left(\frac{GD}{\mu}\right)^{0.8} \left(\frac{c_p \mu}{k}\right)^{0.4} \left(\frac{k}{D}\right) \tag{1}$$

$$h = 0.023 \left(\frac{G^{0.8}}{D^{0.2}}\right)\left(\frac{c_p^{0.4} k^{0.6}}{\mu^{0.4}}\right) \tag{2}$$

The significance of this trend is that, for hydrogen and helium, there is probably a small difference between the heat transfer of liquid to the wall and that of vapor to the wall. This explains why the heat transfer during transition boiling and nucleate boiling, which each contain some amount of liquid-to-wall convection heat transfer, are not that different than the heat transfer during film boiling for the LH_2 chilldown data. As for nitrogen, oxygen, and methane, the data shows a large increase in heat transfer from film boiling to transition and nucleate boiling, which is consistent with the change in the single-phase HTC value from gas to liquid.

Despite its partial success, the GFSSP results with the single-phase Dittus-Boelter correlation overestimated the heat transfer rate and predicted a more rapid chilldown of the pipe wall temperature in all cases, especially at locations far from the pipe inlet. The main reason is that the model in Leclair et al. (2018) does not include the effect of thermal nonequilibrium. Thermal nonequilibrium during flow film boiling occurs when the wall-to-vapor heat transfer exceeds the vapor-to-liquid heat transfer. This causes the vapor to heat to temperatures above the liquid temperature, so that the flow consists of liquid droplets entrained in a warmer vapor flow. Thermal nonequilibrium tends to become significant for flows at medium to high quality in which the volume fraction of vapor is higher than that of the liquid. If thermal equilibrium is assumed, a dispersed flow film boiling correlation generally overpredicts the heat transfer. This is because the temperature difference driving the heat transfer is larger if the saturation temperature is used instead of the actual vapor temperature, i.e. $(T_w - T_v) < (T_w - T_{sat})$. The level of nonequilibrium can

be visualized with a plot of the actual quality, x_a, against the equilibrium quality, x_e. It has been shown for LN_2 pipe flow film boiling that the actual quality can be less than one at equilibrium qualities up to 3, as shown in Figure 2 (Forslund and Rohsenow 1968). The same trend is shown in Groeneveld and Delorme (1976) and Shah and Siddiqui (2000). Chi (1967) measured the stream temperature in LH_2 pipe chilldown experiments and reported vapor temperatures significantly higher than the saturation temperature during film boiling. The film boiling efficiency, defined as the ratio of the liquid-to-vapor heat flux to the wall-to-vapor heat flux, was reported to be as low as 8% for these experiments. The film boiling efficiency was found to increase for increasing actual quality. Therefore, it is expected that the level of nonequilibrium increases as the flow progresses farther from the quenching front.

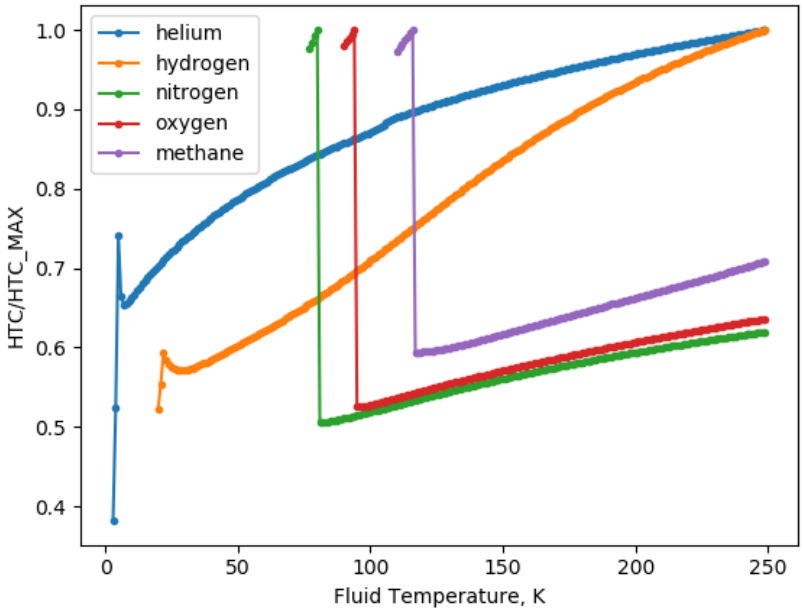

Figure 1. Normalized HTCs, using the Dittus-Boelter single-phase correlation. Liquid properties are used for fluid temperatures below the saturation temperature. Vapor properties are used for fluid temperatures above the saturation temperature. G = 50kg/m^2-s, P = 150kPa, and D = 0.0127 m (1/2in).

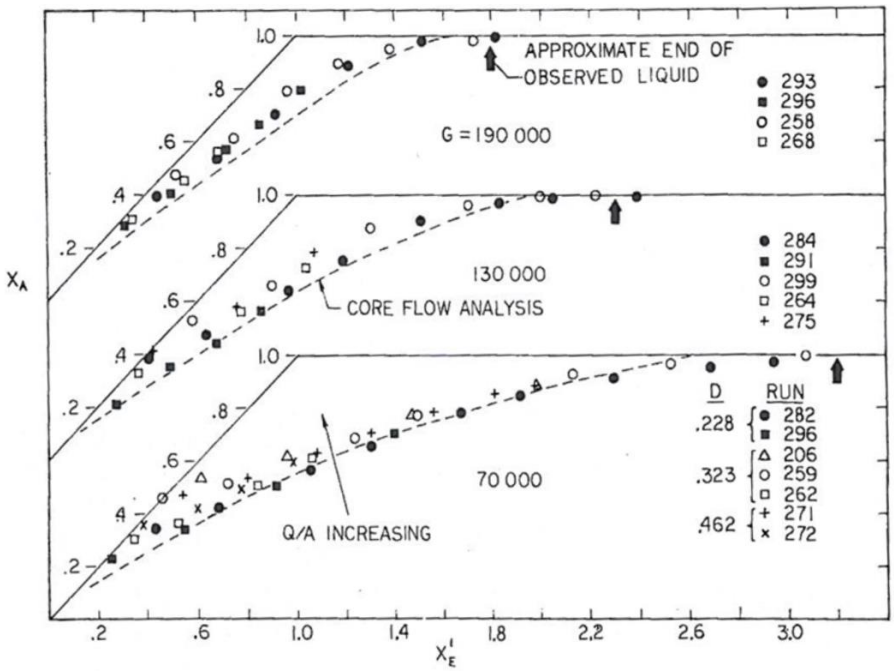

Figure 2. x_a vs. , x_e for LN_2 chilldown, reprinted from Forslund and Rohsenow (1968).

The purpose of current work is to develop a set of LH_2-only correlations that correctly accounts for the effects of thermal nonequilibrium. The correlation set is fit to the LH_2 pipe chilldown experimental data by using a lumped-node heat transfer model to simulate the chilldown of the entire pipe from the inlet to the second wall temperature measurement location. A review of the data, correlations, fitting method, and the comparison of the model to the data is presented below.

2 Experiment Overview

2.1 Experiment Description

Recently, a set of liquid hydrogen transfer line chilldown tests were conducted at the NASA Glenn Research Center. Only a brief description is given here; for a detailed description, the reader is referred to Hartwig et al. (2019). Tests were conducted over a range of mass flow rates (0.0023 – 0.036 kg/s) and liquid saturation temperatures (20.3 K, 21.4 K, 22.9 K, and 24.2 K). Liquid hydrogen was conditioned inside a storage dewar and flow was routed directly to a Coreolis flow meter to measure liquid flow. The tank and line chill assembly rested inside a vacuum chamber (VC) with a thermally controlled cryoshroud that was set to 1.33×10^{-7} Pa and 250K. Fluid was routed vertically upward through a flow control manifold. Orifices were used to control lower and medium flow rates, while the pipe diameter and driving pressure gradient set the higher flow rate limit. Flow was then sent either through a sight glass used to visualize flow as the test evolved, or through a leg that contained a pump mass simulator at the end of the leg. Test results reported here are from the pump leg. Then out of the top of the VC lid. Silicon diodes were used to measure wall mounted temperatures along the transfer line as well as internal stream temperature. Pressure transducers were used to measure inlet and exit pressure. The outer diameter of the transfer line was 1.27 cm (0.5 in) and the inner diameter was 1.02 cm (0.402 in).

2.2 Correlation Development Challenges

A plot of the upstream temperature and wall-to-fluid heat flux vs. time for one of the test runs is given in Figure 3a. The boiling curve (the HTC $h = q''/(T_w - T_{sat})$ instead of the heat flux on the y-axis) for the upstream and downstream locations is shown for the same test, with the mass flux measurement overlaid for reference. For the first 28s, the heat flux is increasing in time. The flow is single-phase vapor at this point, and the increase in heat flux is due to the decrease in the vapor temperature. The local vapor temperature is decreasing in time as more of the pipe is chilled down upstream of the temperature station and less total heat is input into the flow before the flow reaches the temperature station. After 28s, the heat flux begins to decrease. Chi (1967) suggested this transition point as the beginning of film boiling. However, from Figure 1 it is evident that the HTC decreases with vapor temperature. Therefore, the 28s mark could indicate the point at which the decrease in the local HTC outweighs the increase in the wall-fluid temperature difference. So this peak heat flux at 28s does not necessarily signify the presence of liquid in the flow.

Another dividing point in the heat flux curve is at 46s. At this point, there is a rise in the heat flux, and the heat flux becomes noisier. At first glance of Figure 3b at this location, when referencing a typical boiling curve, this appears to signify the Leidenfrost temperature and the incipience of transition boiling. However, the wall temperature of 120 K is much higher than the theoretical superheat limit of hydrogen, estimated to be 28 K (see Darr et al. 2019b for equation). Thus, it is unlikely that transition boiling, which is a mixture of nucleate boiling and film boiling, can occur at this high of a surface temperature. As an example, only modest increases in the Leidenfrost point of 5 K to 30 K above the theoretical superheat limit of nitrogen have been recorded for pipe chilldown (Darr et al. 2019b). Another candidate for this transition point is the introduction of relatively large liquid slugs in the flow. LH_2 chilldown data from Chi (1967) showed measured stream temperatures sporadically dropping from warm vapor temperatures to the liquid temperature only after the wall temperature fell below 125 K. These transitory spikes to the liquid temperature were indicative of liquid slugs entering the flow. This did not necessarily indicate transition boiling, but instead indicated something like a temporary inverted annular flow (IAF) pattern. More support for this interpretation is provided by the flow visualization data from the NASA GRC LH_2 chilldown tests. These videos showed single-phase gas flow until the sight-glass wall temperature reached 115 K, in which mist flow was observed. Then, at a wall temperature of 70 K the first slug flow patterns were observed. Liquid contact with the wall, which is required for nucleate boiling, was not observed until the wall temperature reached 40 K. Based on this information, it is most likely the case that the single-phase vapor convection occured for the first 28s, from 28s to 46s the flow was either single-phase vapor or mist flow, from 46s to 59s the heat transfer was enhanced by slug flow, and at around 59s the liquid began to contact the wall.

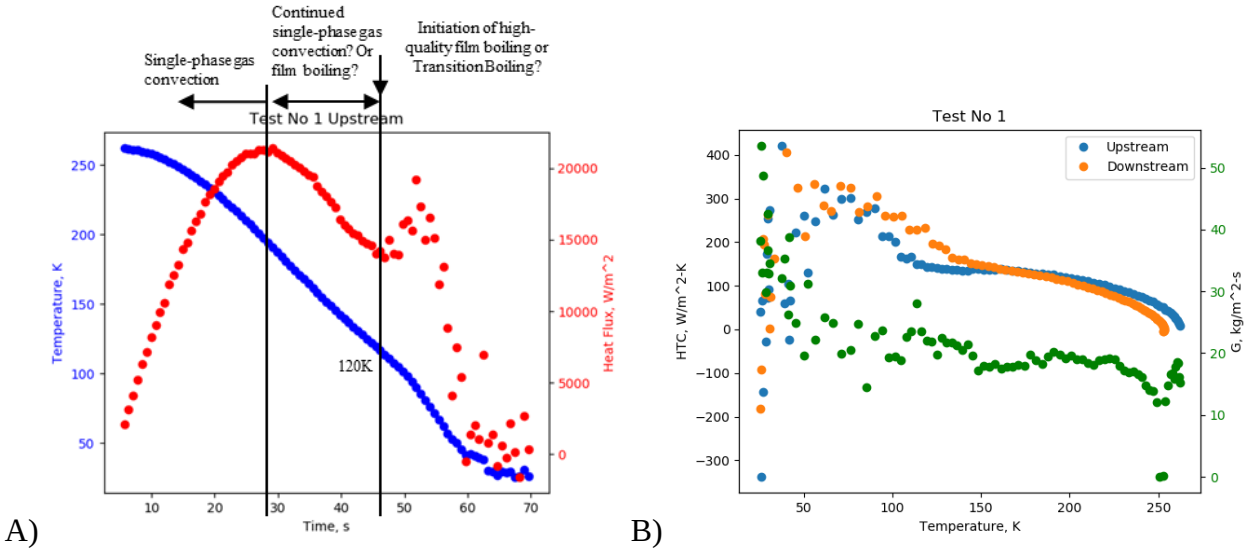

Figure 3. LH_2 pipe chilldown test data at low mass flux. A) Temperature and heat flux at the upstream location as a function of time. B) HTCs for the upstream and downstream location and mass flux as a function of wall temperature.

For comparison, Figure 4 shows the same plots for a test at a higher mass flux. At this higher mass flux, the pipe cools down to the liquid temperature at a much faster rate. The data sampling rate is too small to detect minor changes in the heat flux. Yet, the same trend in the boiling curve as in Figure 3b appears in Figure 4b.

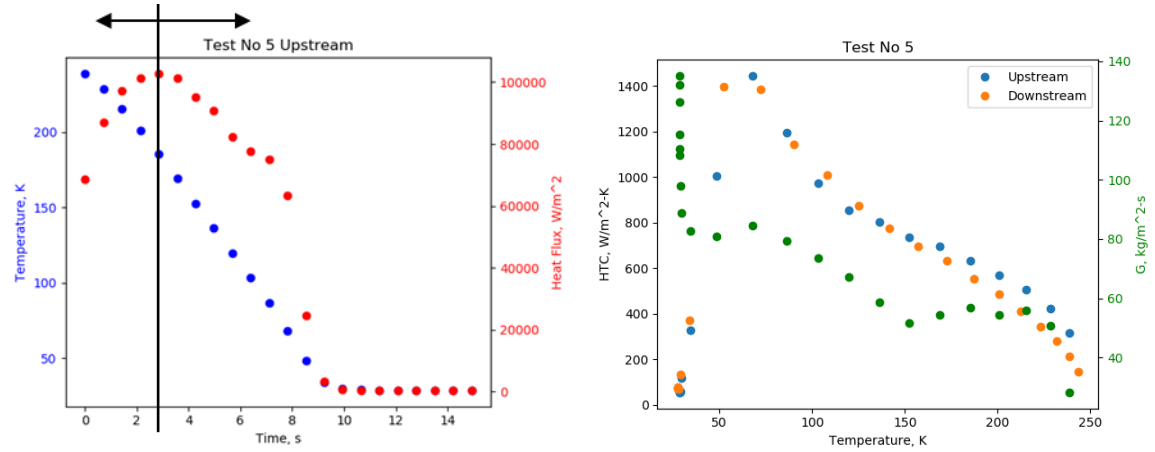

Figure 4. LH_2 pipe chilldown test data at high mass flux. A) Temperature and heat flux at the upstream location as a function of time. B) HTCs for the upstream and downstream location and mass flux as a function of wall temperature.

Another major challenge in developing correlations with the current LH_2 chilldown data is that the fluid stream temperature is unknown along the distance of the tube. The fluid temperature during chilldown for most of the test is superheated well above the saturation temperature, but there are no fluid temperature measurements at the local wall temperature locations. The wall temperature data is taken at locations relatively far downstream at 14.5 and 50 inches from the

inlet, where almost all data is for either single-phase vapor convection or mist flow with high amounts of thermal nonequilibrium. This is in contrast with the LN_2 data from Darr et al. (2016b) which obtained measurements at shorter distances (5 and 15 inches), which, combined with the higher mass fluxes tested and the fact that more energy is required to boil off the LN_2, resulted in vapor temperatures much closer to the saturation temperature.

One consequence of unknown fluid temperatures is that the NASA LH_2 chilldown data cannot be used in a direct way to develop a correlation at the locations near the inlet or the quenching front. At these locations, the vapor mass fraction is small and the wall superheat, $T_w - T_v$, is large. This is unlike the case at the locations of the wall temperature measurements downstream where the vapor mass fraction is large and the wall superheat is small. Applying the dispersed flow film boiling or single-phase vapor correlation that was developed from the data to the upstream locations causes an error in the prediction. A separate correlation, one developed for slug flow or IAF, is needed for the locations near the inlet. This type of correlation is presented later in the paper.

Another consequence for the LH_2 chilldown data is that the quality of the flow at the local wall temperature measurements is not easily estimated. The equilibrium quality extrapolation method that was used for LN_2 data was sufficient in that case because wall temperature measurements were taken close to the inlet where the flow regime was IAF. There is no knowledge of the how the heat flux varies near the inlet for the LH_2 chilldown data.

Because of the difficulties mentioned above in determining the flow regime, the fluid temperature, and the equilibrium quality, a different approach is needed to develop the new heat transfer correlation set from the LH_2 chilldown data. This approach, which involves performing a simulation with a numerical model of the heat transfer along the tube, is discussed in the next section.

3 Pipe Chilldown Model

3.1 Approach to fitting correlations

To address the problems mentioned in section 2.2, the following approach was taken to fit the heat transfer correlations. A lumped-node heat transfer model was used to simulate the chilldown of the entire pipe from the inlet to the second wall temperature measurement location. A set of correlations for the film boiling, transition boiling, nucleate boiling heat flux was used to predict the wall-to-fluid heat transfer. Correlations for the Leidenfrost temperature and critical heat flux were used to determine dividing points between the boiling regimes. A correlation was employed to estimate the thermal nonequilibrium of the flow. Different historical correlations in the literature were attempted to determine the best functional form that fit the data. The resulting transient wall temperature predicted by the model was compared to the LH_2 chilldown data at the corresponding measurement locations. A generic numerical optimization technique was used to fit the constants of the correlations to minimize the error against the data.

3.2 Heat transfer correlations

3.2.1 Film boiling and single-phase vapor

The film boiling and single-phase vapor heat transfer correlations are the main thrust of this paper because the majority of time for LH_2 chilldown is spent in these regimes. Pipe flow film boiling correlations have historically been divided into two regimes: IAF film boiling and dispersed flow film boiling. IAF generally occurs immediately downstream of the quenching front, where the quality of the flow is close to zero. A liquid core passes through the center of the pipe and a vapor annulus surrounds this liquid core, separating it from the wall. Liquid evaporates from the core surface as the flow progresses down the pipe, thinning the diameter of the liquid core. As the core thins, it breaks into slugs of liquid that can be separated by vapor gaps. Continuing downstream, the slugs decrease in size until the flow consists of droplets entrained in a vapor flow. This regime is dispersed flow film boiling.

In IAF, the heat transfer is generally larger when the vapor annulus is thinner. A thinner vapor annulus has the effect of increasing the vapor temperature gradient at the wall. This drives the trend that IAF film boiling heat transfer is larger for smaller qualities. In dispersed flow, the opposite is true. As the liquid droplets reduce in size and quantity, the speed of the vapor increases for the same given mass flux. This produces higher convection heat transfer at the wall. However, in some cases, especially at high mass fluxes, it has been shown that droplets can influence the heat transfer during dispersed flow film boiling. This effect will be ignored in this paper since the mass fluxes for the LH_2 chilldown data are relatively small. Above some quality in dispersed flow film boiling, thermal nonequilibrium will begin to degrade the heat transfer. The vapor warms at a faster rate than it would in nonequilibrium, and this lowers the wall superheat that drives the heat transfer. Additionally, there is more liquid present in nonequilbrium than in equilibrium, which lowers the vapor velocity.

The difference in the flow patterns of IAF and dispersed flow make it difficult to develop a single correlation that accurately predicts the heat transfer in both regimes. Therefore, the approach in this paper is to develop a separate correlation for each regime and join them together by the *p*-norm method to provide a single film boiling correlation.

The dispersed flow film boiling correlation is similar to those developed by Rohsenow (1988) and Groeneveld and Delorme (1976). The advantage of this correlation is it has successfully predicted the thermal nonequilibrium for multiple fluids, including LN_2. The correlation, which is dominant at medium to high qualities, takes the following form:

$$Nu_{DF} = c_1 Re_{tp}^{c_2} Pr_{v,f}^{c_3} \tag{3}$$

In the equation above, the droplet heat transfer enhancement term that is present in the Rohsenow correlation is neglected. The two-phase vapor Reynolds number is defined as:

$$Re_{tp} = \frac{G x_a D}{\mu_{v,f} \alpha} \tag{4}$$

The void fraction, α, assumes the slip ratio is equal to 1.

$$\alpha = \left[1 + \frac{\rho_v}{\rho_{l,sat}}\left(\frac{1-x_a}{x_a}\right)\right]^{-1} \tag{5}$$

The vapor density is taken at the bulk vapor temperature and local pressure.

The form of the film boiling convection term in the correlation in Darr et al. (2016b) and Darr et al. (2019a) is used to represent the heat transfer during IAF and slug flow, which is dominant at low qualities:

$$Nu_{IAF} = c_4 \frac{D}{k_{v,sat}}\left[\frac{\rho_{v,sat}\left(\rho_{l,sat}-\rho_{v,sat}\right)g h_{fg} k_{v,sat}^3}{L\mu_v(T_w - T_{sat})}\right]^{1/4} + c_5(1-x_a)^{c_6} Re_v^{c_7} Pr_v^{c_8} \tag{6}$$

This correlation was developed originally from LN_2 data at qualities in the range of −0.13 to 0.4, with a majority of the data at qualities near zero or negative. In this regime, the relationship between the convection heat transfer and the quality is different than it is for high qualities. This difference is owed to the flow patterns at low and high qualities. At low qualities, the higher volume of liquid present in the flow forms an IAF pattern, in which a liquid core is surrounded by a vapor annulus that is contacting the wall. At high qualities, the liquid is in the form of small liquid droplets that are entrained in the vapor flow. In the low-quality regime, decreasing the quality further causes the vapor annulus to decrease, effectively decreasing the thermal boundary layer at the wall. In the high-quality regime, as the quality is increased, the heat transfer will also increase due to the increase in the vapor velocity. The liquid droplets have little influence over the heat transfer at the wall, and at higher qualities, the speed of the vapor is increased for a given mass flux. The higher vapor speed generates higher convection heat transfer at the wall. This relationship is captured in Figure 5, which plots the heat flux for the low- and high-quality regimes, as well as the combined value, against the equilibrium quality for example hydrogen chilldown conditions. The value of c_6 in Eq. (6) is some positive number so that the Nu number increases as quality decreases.

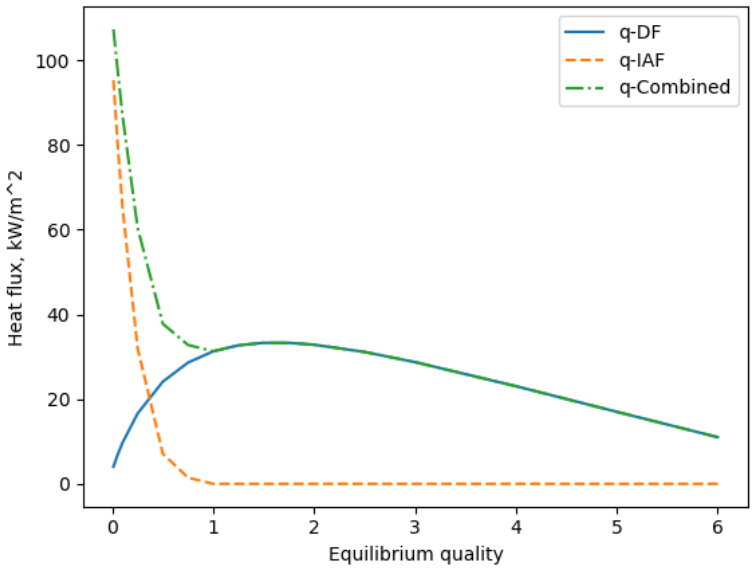

Figure 5. Breakdown of the heat fluxes, including the high quality, i.e. dispersed flow, heat flux (q-DF) and the low quality, i.e. inverted annular flow, heat flux (q-IAF). The calculation uses an example hydrogen chilldown scenario with a mass flux of 20 kg/m^2-s, pressure of 200 kPa, wall temperature of 250 K.

Lastly, a correlation is required to predict the actual quality, which determines the extent of thermal nonequilibrium. Historically, correlations for actual quality were developed for heated tube and assume a constant wall heat flux across the entire tube length (Rohsenow 1988, Groeneveld and Delorme 1976). In these correlations, the actual quality is a function of the applied heat flux. This method of correlation is unsuitable for quenching, in which the heat flux is unknown and is part of the solution. Shah and Siddiqui (2000) provide a correlation for actual quality as a function of equilibrium quality and Froude number. A similar approach will be taken in this paper. However, the Reynolds number will be used instead of the gravity-dependent Froude number so that the correlation can be extended to different flow directions and a zero gravity environment. The explicit equation below is used to find the actual quality:

$$x_a = \left(\frac{1}{x_e^K} + 1\right)^{-1/K} \tag{7}$$

This follows a similar trend found in the LN_2 data by Forslund and Rohsenow (1968), as indicated by Figure 6. The value of K is a function of the liquid Re number, and should be higher for larger Re_l. A linear relationship between K and Re_l was determined to be sufficient.

$$K = c_9 Re_l + c_{10} \tag{8}$$

The bulk vapor temperature corresponding to the actual quality can then be found from:

$$T_v = \left(\frac{x_e - x_a}{x_a}\right)\frac{h_{fg}}{c_{p,v}} + T_{sat} \tag{9}$$

The vapor specific heat, $c_{p,v}$, does not change significantly with temperature for LH_2, so the value is taken at the saturated vapor condition corresponding to the local pressure. This helps to avoid having to iteratively solve the equation for the vapor temperature.

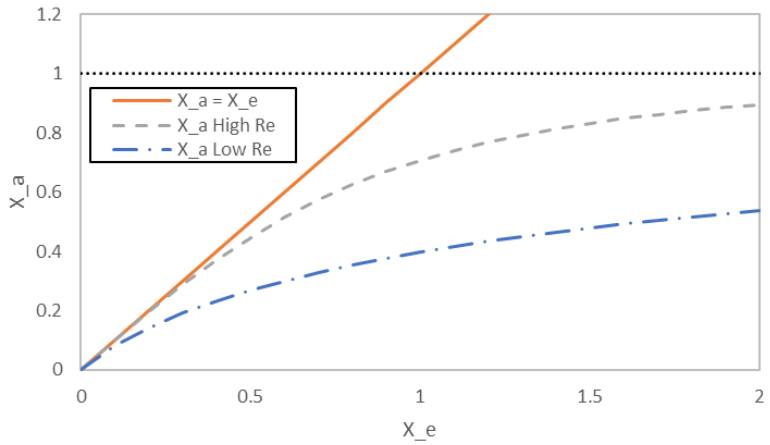

Figure 6. Actual quality vs. equilibrium quality. Two separate curves of Eq. (8) are shown, one to represent a high mass flux case (K = 2) and the other to represent a low mass flux case (K = 0.75).

The p-norm is applied to the low- and high-quality Nu numbers to obtain a single value for the correlation. The value of p, which determines how the Nu number transitions from one region to the other, is an additional parameter to fit to the data.

$$Nu_{FB} = \left(Nu_{IAF}^{p} + Nu_{DF}^{p}\right)^{1/p} \tag{10}$$

There are quality-dependent conditions on the Nusselt numbers. If $x_e < 0$, then Nu_{DF} is set to 0. If $x_e > 1$, then Nu_{IAF} is set to 0. Also, if $x_a > 0.99$, then x_a is set equal to 1, and the heat transfer mechanism is single-phase vapor convection. This last condition must be implemented because with the proposed correlation for x_a, the value of x_a will never reach one, no matter how large x_e becomes.

The HTC and heat flux are calculated from the Nu number by the following:

$$\frac{q''_{FB}}{T_w - T_v} = h_{FB} = \frac{k_{v,sat}}{D} Nu_{FB} \tag{11}$$

The coefficients $c_1 - c_{10}$ and p are fit to the data using the method discussed in the previous section.

In the event that the $x_a > 0.99$, the correlation automatically simplifies to a single-phase vapor correlation automatically.

$$Nu_{SP} = Nu_{FB}(x_a = 1) = c_1 \left(\frac{GD}{\mu_{v,f}} \right)^{c_2} Pr_{v,f}^{c_3} \tag{12}$$

This approach ensures that the heat flux transitions smoothly from the film boiling regime to the single-phase vapor regime, and vice versa.

3.2.2 Nucleate boiling

As addressed in Hartwig et al. (2016), most nucleate boiling correlations are developed for heated tube data and use some form of the boiling number in the correlation. This approach is unsuitable for a quenching application, since the heat flux is an unknown value. Darr et al. (2016b) presented a nucleate boiling correlation for LN_2 data in the following form for upward flow:

$$h_{NB} = 61.6 Re_l^{-.332} Ja_l^{-.254} h_{DB} \tag{13}$$

The Dittuse-Boelter correlation for liquid flow is expressed as:

$$h_{DB} = 0.023 Re_l^{0.8} Pr_l^{0.4} \left(\frac{k_l}{D} \right) \tag{14}$$

The Jakob number is:

$$Ja_l = \frac{c_{pl}(T_w - T_{sat})}{h_{fg}} \tag{15}$$

The heat flux is then found from:

$$q''_{NB} = h_{NB}(T_w - T_{sat}) \tag{16}$$

This correlation gives values ranging from 5 to 10 kW/m^2 for the LH_2 chilldown dataset at the maximum expected DNB temperature of 2K. This compares well with carefully controlled heated tube experiments in Shirai et al. (2011).

3.2.3 Transition boiling

Transition boiling is a mixture of film boiling and nucleate boiling. When the wall temperature is above the DNB temperature but below the Leidenfrost temperature, the flow is in the transition boiling regime. The range of wall temperatures that the flow is in transition boiling is small, so the time spent during transition boiling is brief for pipe childown. It is difficult to determine from the data the exact transition boiling heat flux due to aliasing of the data. Therefore, a simple linear fit from $q''_{NB}(T_{DNB})$ to $q''_{FB}(T_{Wet})$ is used to find the transition boiling at a given wall temperature.

$$q''_{TB}(T_w) = [q''_{NB}(T_{DNB}) - q''_{FB}(T_{wet})] \left(\frac{T_w - T_{wet}}{T_{DNB} - T_{wet}} \right) + q''_{FB}(T_{wet}) \tag{17}$$

3.2.4 Leidenfrost temperature

The exact Leidenfrost temperature is difficult to determine from the LH_2 chilldown data, as mentioned earlier. The correlation for the Leidenfrost temperature is taken from Darr et al. (2019b), ignoring the effects of the transient solid surface temperature and the surface energies which are minor for stainless steel and hydrogen. This correlation was fit to LN_2 data but gives reasonable values of 31 K to 33 K for hydrogen depending on the mass flux and the local pressure.

$$T_{wet} = 0.844T_{cr}(1 + 0.060We_D^{0.208}) \tag{18}$$

3.2.5 Temperature at the departure from nucleate boiling

The departure from nucleate boiling (DNB) temperature and heat flux were measured by Shirai et al. (2011) for LH_2 during heated tube experiments for a relatively high pressure of 700 kPa. The value of the DNB temperature was heavily dependent on the liquid subcooling at the inlet and the mass flux. For saturated liquid at the inlet, the DNB temperature was approximately 2 K above the saturated temperature for a cross-section averaged liquid velocity of 1.33 m/s. This was the lowest mass flux tested in the experiment. The liquid velocity for the current LH_2 chilldown experiment ranged from approximately 0.2 to 0.8 m/s. Therefore, the maximum expected DNB temperature is expected to be 2 K above T_{sat}. Above this temperature the flow is in transition boiling.

$$T_{DNB} - T_{sat} = 2 \tag{19}$$

3.3 Model Description

The numerical model that was used to simulate the pipe chilldown was presented in Darr et al. (2015). Details are given in that paper, and a brief description is given here. The test section was divided into evenly-spaced, lumped-parameter nodes and the finite volume technique was used to solve the transient energy equation in the axial direction of the solid pipe. It was assumed that the temperature gradients in the radial and azimuthal directions were negligible in comparison to the gradients in the axial direction. This assumption is appropriate for thin tubes like the one used for the LH_2 chilldown tests where axial conduction is only relevant at the quenching front (Kawanami et al. 2007). The heat flux correlations were applied to the inner surface of each node depending on the local fluid conditions at the given node. The continuity and momentum equations for the fluid were not solved. Instead, the transient measured mass flux was used for each node at each timestep. It was assumed that the mass flux at the flow meter was equal to the mass flux over the entire pipe. There is some error with this method, but it is small as has been shown with simulations using commercial lumped-node solvers. Linear interpolation of the transient pressure measurements at the inlet and exit of the test section was used to estimate the local pressure at each node and timestep. This approach of using the measured mass flux and pressure measurements was chosen to provide the most accurate fluid conditions to the model, and avoid the error introduced by solving the fluid continuity and momentum equations. In this way, this would keep the main focus on the evaluation of the heat transfer correlations. The energy equation had to be solved for the fluid next to each solid node at each timestep to determine the fluid temperature and equilibrium quality to be used in the correlations for each node. This method is discussed in more detail in Darr et al. (2015).

Radiation and gas conduction from the surroundings outside the test section tube made up the parasitic heat and were estimated for the simulation. A central difference scheme was used for the second-order spatial derivative and the first-order, fully-implicit time integration method was used. A tridiagonal matrix solver was used to solve the equations set at each timstep. A convergence study was performed on both the number of nodes and the timestep. 40 nodes and a timestep of 0.01s were found to be sufficient.

The logic to determine what correlation to use – either single-phase vapor, film boiling, transition boiling, or nucleate boiling – for the local fluid and wall conditions went as follows:

- Calculate T_{wet} for the mass flow rate and local pressure at the node
  - If $T_w > T_{wet}$ then calculate x_a from the thermal nonequilibrium correlation
    - If $x_a < 0.99$, $q'' = q''_{FB}$
    - If $x_a \geq 0.99$, set $x_a = 1$, $q'' = q''_{SP} = q''_{FB}(x_a = 1)$
  - If $T_w \leq T_{wet}$, then:
    - If $T_w > T_{DNB}$, $q'' = q''_{TB}$
    - If $T_{wet} \leq T_{DNB}$, $q'' = q''_{NB}$

4 Results

4.1 Finalized correlation set

The correlation set is presented in Table 1 with the finalized constants c_1-c_{10} and p.

Table 1. Correlation set with final coefficients.

Parameter	Correlation
x_a	$x_a = \left(\frac{1}{x_e^K} + 1\right)^{-1/K}$ $K = 5.26 \times 10^{-5} Re_{l,in} + 0.11$
q''_{fb}	$q''_{FB} = Nu_{FB} k_{v,sat}(T_w - T_v)/D$ $Nu_{FB} = \left(Nu_{IAF}^{3/4} + Nu_{DF}^{3/4}\right)^{4/3}$ $Nu_{DF} = 0.015 Re_{tp}^{0.8774} Pr_{v,f}^{0.6112}$ $Nu_{IAF} = 0.06 \left[\frac{\rho_{v,sat}(\rho_{l,sat} - \rho_{v,sat}) g h_{fg} k_{v,sat}^3}{L \mu_g (T_w - T_{sat})}\right]^{1/4} + 0.015(1 - x_a)^4 Re_v^{0.8} Pr_{v,sat}^{0.8}$
q''_{NB}	$q''_{NB} = h_{NB}(T_w - T_{sat})$ $h_{NB} = 61.6 Re_l^{-.332} Ja_l^{-.254} h_{DB}$ $h_{DB} = 0.023 Re_l^{0.8} Pr_l^{0.4} \left(\frac{k_l}{D}\right)$
q''_{TB}	$q''_{TB}(T_w) = [q''_{NB}(T_{DNB}) - q''_{FB}(T_{wet})] \left(\frac{T_w - T_{wet}}{T_{DNB} - T_{wet}}\right) + q''_{FB}(T_{Wet})$
T_{wet}	$T_{wet} = 0.844 T_{cr}(1 + 0.060 We_D^{0.208})$
T_{DNB}	$T_{DNB} = 2K$

4.2 Comparison with data

The model wall temperature prediction is compared to the test data for three tests which represent low (Figure 7A and B), medium (Figure 7C and D), and high flow rate (Figure 7E and F) tests for the pump simulator leg. The average mass flux, G_{avg}, for each test was 21, 38, and 81 kg/m^2-s, respectively. For each test, the chilldown curve (T_w vs. time) and the boiling curve (q''_w vs. T_w) of the model is compared to the data. The model has better overall agreement at higher mass fluxes. At lower mass fluxes, it tends to over-predict the heat flux near the beginning of chilldown. Analysis of the data suggests that the amount of nonequilibrium is underestimated by the correlation for actual quality. Attempts were made to improve this prediction at low mass fluxes but were unsuccessful.

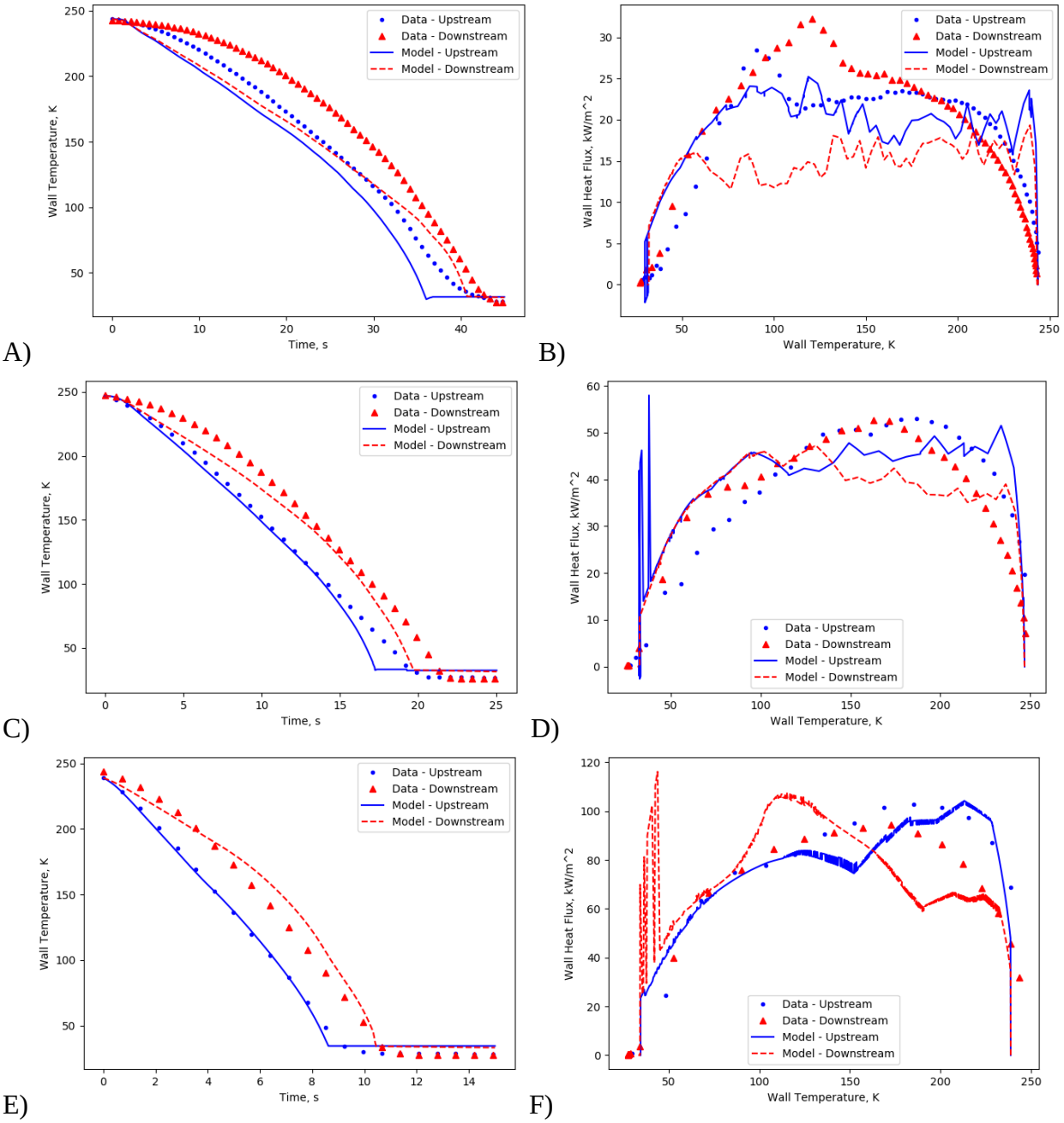

Figure 7. Comparison of the model vs. the data. On the left side are the chilldown curves, on the right side are the corresponding boiling curves. A) and B) are the chilldown and boiling curves, respectively, for the low mass flux test, G_{avg} = 21 kg/m^2-s. C) and D) are the chilldown and boiling curves, respectively, for the medium mass flux test, G_{avg} = 38 kg/m^2-s. E) and F) are the chilldown and boiling curves, respectively, for the high mass flux test, G_{avg} = 81 kg/m^2-s.

The mean absolute error (MAE) was calculated for the wall temperature at the two temperature measurement locations for ten of the twelve LH_2 chilldown tests on the pump leg, a total of 506 data points, where MAE is defined as

$$\mathrm{MAE} = \frac{1}{N}\sum_{i=1}^{N} |\mathrm{data}(t_i) - \mathrm{model}(t_i)| \tag{20}$$

where N is the number of data points, and t_i is the time corresponding to each data point. The MAE averaged over all tests for both locations, was found to be 19.5 K. Two of the tests were left out because the pipe began at a non-uniform temperature initial condition. These results are a 40% improvement over the results from Leclair et al. (2018), which obtained a MAE value of 32.7 K when averaged for both temperature locations over all tests that were simulated in that paper using GFSSP with the correlation set from Darr et al. (2019a).

5 Conclusion

A new correlation set, implemented in a numerical heat transfer model, was able to predict the transient wall heat flux and wall temperature with improved accuracy over existing correlations for the chilldown of a vertical pipe with LH_2 flowing upward. These results support the validity of the correlation for the actual quality (i.e. nonequilibrium), the heat transfer correlations for all three of the boiling regimes, the correlations for the dividing points of the boiling regimes (the Leidenfrost temperature, and the DNB temperature), as well as the logic employed when choosing which correlation to use under local conditions. These correlations can be used to improve the accuracy of commercial software packages when simulating LH_2 transfer line chilldown.

Acknowledgements

Thanks to Dr. Matthew Taliaferro for the discussions on *p*-norms, and his generosity in developing a functional form for the actual quality.

This work was funded by the Nuclear Thermal Propulsion project at NASA Glenn Research Center under NASA contract #NNJ11HB94C.

References

Chi, J.W.H., Vetere, A.M., "Two-phase flow during transient boiling of hydrogen and determination of nonequilibrium vapor fractions" *Advances in Cryogenic Engineering* 9, 243-253. 1964.

Chi, J.W.H., "Slug flow and film boiling of hydrogen" *Journal of Spacecraft and Rockets* 4(10), 1329-1332. 1967.

Darr, S.R., Hu, H., Glikin, N., Hartwig, J.W., Majumdar, A.K., Leclair, A.C., Chung, J.N. "An experimental study on terrestrial cryogenic tube chilldown I. Effect of mass flux, equilibrium quality, and inlet subcooling" *International Journal of Heat and Mass Transfer* 103, 1225-1242. 2016a.

Darr, S.R., Hu, H., Glikin, N., Hartwig, J.W., Majumdar, A.K., Leclair, A.C., Chung, J.N. "An experimental study on terrestrial cryogenic tube chilldown II. Effect of flow direction with respect to gravity and new correlation set" *International Journal of Heat and Mass Transfer* 103, 1243-1260. 2016b.

Darr, S.R., Hartwig, J.W., Dong, J., Wang, H., Majumdar, A.K., Leclair, A.C., Chung, J.N. "Two-phase pipe quenching correlations for liquid nitrogen and liquid hydrogen" *Journal of Heat Transfer* 141(4). 2019a.

Darr, S.R., Dong, J., Glikin, N., Hartwig, J.W., Chung, J.N., "Rewet temperature correlations for liquid nitrogen boiling pipe flows across varying flow conditions and orientations" *Journal of Thermal Science and Engineering Applications* 11(5), 2019b.

Forslund, R.P., Rohsenow, W.M. "Dispersed flow film boiling" *Journal of Heat Transfer* 90(4), 399-407. 1968.

Groeneveld, D.C., Delorme, G.G.J. "Prediction of thermal non-equilibrium in the post-dryout regime" *Nuclear Engineering and Design* 36, 17-26. 1976.

Hartwig, J.W., Darr, S.R., Asencio A. "Assessment of existing two phase heat transfer coefficient and critical heat flux correlations for cryogenic flow boiling in pipe quenching experiments" *International Journal of Heat and Mass Transfer* 93, 441-463. 2016.

Hartwig, J.W. and Styborski, J. "Flow Visualization and Stream Temperature Measurement of Liquid Hydrogen Line Chill Down Experiments" *HT-14-1606, ASME Journal of Heat Transfer* 137, Issue 2, 020904, February 1, 2015.

Hartwig, J.W., Styborski, J., McQuillen, J., Rame, E., Chung, J. "Liquid Hydrogen Line Chilldown Experiments: Optimal Chilldown Methods" *International Journal of Heat and Mass Transfer* 137, 703 – 713. 2019.

Jin, L., Cho, H., Lee, C., and Jeong, S. "Experimental research and numerical simulation on cryogenic line chill-down process" *Cryogenics* 89, 42 – 52. 2018.

Kawanami, O., Nishida, T., Honda, I., Kawashima, Y., and Ohta, H. "Flow and Heat Transfer on Cryogenic Flow Boiling during Tube Quenching under Upward and Downward Flow" *Microgravity Science and Technology* 9.3 – 4, 137 – 138. 2007.

Leclair, A., Hartwig, J.W., Hauser, D.M., Kassemi, M., Diaz-Hyland, P.G., Going, T.R. "Modeling cryogenic chilldown of a transfer line with the Generalized Fluid System Simulation Program" *Joint Propulsion Conference*, 9-11 July 2018.

Rohsenow, W.M. "Post dryout heat transfer prediction method" *International Communications in Heat and Mass Transfer* 15, 559-569. 1988.

Sakowski, B., Hauser, D.M., Hartwig, J.W., Kassemi, M. "Validation of heat transfer correlations in line chill-down tests of cryogenic fluid in SINDA/FLUINT" *International Energy Conversion Engineering Conference*, 9-11 July 2018.

Shah, M.M., Siddiqui, M.A., "A general correlation for heat transfer during dispersed-flow film boiling in tubes" *Heat Transfer Engineering* 21, 18-32. 2000.

Singh, G.K., Pradhan, S., and Tanna, V. "Experimental studies of two phase flow characteristics and void fraction predictions in steady state horizontal two-phase nitrogen flow" *Cryogenics* 100, 77 – 84. 2019.

Shirai, Y., Tatsumoto, H., Shiotsu, M., Hata, K., Kobayashi, H., Naruo, Y., Inatani, Y., Kinoshita, K. "Forced flow boiling heat transfer of liquid hydrogen for superconductor cooling" *Cryogenics* 51, 295-299. 2011.

Vitae

Dr. Samuel Darr is a fluid mechanics analyst at The Aerospace Corporation, where he performs fluid mechanics and heat transfer analysis for multiple launch vehicles. His areas of focus include cryogenic phase change, tank thermodynamic analysis, computational fluid dynamics simulations, two-phase pipe flow boiling, reduced gravity propellant management with surface tension devices, and waterhammer analysis. Sam received his B.S., M.S., and PhD in Aerospace Engineering at the University of Florida. As a postdoctoral researcher and PhD student at the University of Florida, he led experimental and analytical research efforts in propellant management devices and reduced

gravity two-phase cryogenic pipe chilldown. His publications include 10 journal and conference papers on propellant management devices and 9 journal and conference papers on two-phase cryogenic pipe chilldown.

Dr. Jason Hartwig is a research aerospace engineer, liquid propulsion systems, in the Cryogenics branch at the NASA Glenn Research Center in Cleveland, OH. Jason received his B.S. in Physics at John Carroll University, his M.S. in Mechanical Engineering from Case Western Reserve University under the prestigious Case Prime Fellowship, and his PhD in Aerospace Engineering from Case in 2014. Jason has 11 years of experience in cryogenic engineering, with a focus on liquid acquisition devices, transfer line and tank chill and fill methods, tank pressurization systems, multi-layer insulations systems, and superconducting hybrid electric aircraft. He is currently the principle investigator of the Reduced Gravity Cryogenic Transfer project.